analytical chemistry

pubs.acs.org/ac Article

Development of a CRISPR-Cas-Based Biosensor for Rapid and Sensitive Detection of 8-Oxoguanine DNA Glycosylase

Qian Zhang,[§] Shuangnan Zhao,[§] Xiaorui Tian,[§] Jian-Ge Qiu,* and Chun-yang Zhang*

Cite This: *Anal. Chem.* 2022, 94, 2119−2125 Read Online

ACCESS | Metrics & More | Article Recommendations | Supporting Information

ABSTRACT: 8-Oxoguanine DNA glycosylase is essential for maintaining genomic integrity and stability, while its abnormal activity may lead to the disturbance in the normal DNA damage repair and the occurrence of carcinogenicity and teratogenicity. Herein, we construct a CRISPR-Cas-based biosensor for rapid and sensitive measurement of 8-oxoguanine DNA glycosylases. This biosensor involves a hairpin probe and integrates quadratic strand displacement amplification (SDA) with a CRISPR/Cas12a effector with the characteristics of rapidity (within 40 min) and isothermal assay. The presence of 8-oxoguanine DNA glycosylase can initiate the quadratic SDA to produce large amounts of activators with the assistance of polynucleotide kinase (PNK). Subsequently, the activators can bind with crRNA to activate Cas12a, cleaving signal probes and recovering Cy5 fluorescence, which can be accurately quantified by single-molecule imaging. Notably, the designed hairpin probes can effectively block the hybridization of the generated activators with free hairpin probes, endowing this biosensor with high sensitivity. In addition, the utilization of PNK instead of apurinic/apyrimidinic endonuclease (APE1) greatly simplifies the experimental procedure to only a one-step reaction. The introduction of a single-molecule detection further reduces the sample consumption and improves the sensitivity. This biosensor displays a detection limit of 4.24×10^{-9} U μL^{-1}, and it can accurately quantify cellular human 8-oxoguanine DNA glycosylase at a single-cell level. Furthermore, this biosensor can be applied for the screening of inhibitors, the analysis of kinetic parameters, and the discrimination of cancer cells from normal cells, with potential applications in molecular diagnostic and point-of-care testing.

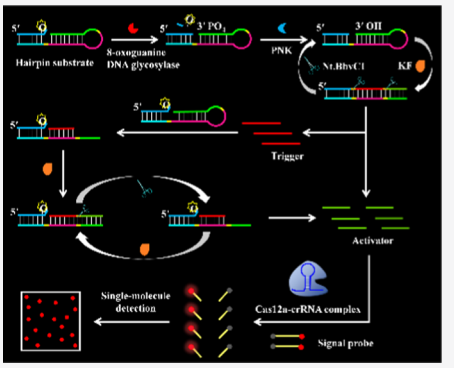

Reactive oxygen species produced by exogenous oxidative stress and endogenous aerobic metabolism may induce oxidative DNA damage (e.g., various base lesions and DNA strand breaks).[1−3] The accumulation of oxidative DNA damage and its mutagenic effects can cause genome instability, premature aging, and carcinogenesis progression.[4] 8-Oxo-7,8-dihydroguanine (8-oxoG) can induce permanent transversion mutation from G:C to T:A by pairing with 2′-deoxyadenosine (dA) during DNA replication.[5] In prokaryotic and eukaryotic cells, 8-oxoguanine DNA glycosylase can initiate a base excision repair (BER) pathway to excise 8-oxoG from 8-oxoG:C base pairs. Aberrant expression of human 8-oxoguanine DNA glycosylase (hOGG1) may induce BER dysfunction, resulting in various human diseases such as Parkinson's disease,[6] autoimmune disease,[7] and different types of cancers (e.g., breast,[8] lung,[9] orolaryngeal,[10] colon,[11] and gastric cancers[12]). Thus, hOGG1 is a valuable biomarker for clinical diagnosis. Formamidopyrimidine [fapy]-DNA glycosylase (Fpg) exists in bacteria and has become a model to study the structural biology and biochemistry of 8-oxyguanidine DNA glycosylases.[13,14] However, a universal biosensor with the capability of detecting both Fpg and hOGG1 has not been reported so far.

The traditional methods for DNA glycosylase assay include radioisotope labeling,[15] mass spectrometry,[16] enzyme-linked immunoassay,[17] and high-performance liquid chromatography,[18] but they suffer from hazardous radiation, expensive antibodies, complex sample preparation, and poor sensitivity. Alternatively, some signal amplification strategies (e.g., exonuclease III-assisted isothermal amplification,[19] loop-mediated isothermal amplification (LAMP),[20] and rolling circle amplification (RCA)[21]) have been introduced to sensitively detect 8-oxoguanine DNA glycosylase. However, they involve complex probe design, multiple time-consuming steps (more than 500 min),[21] and a false-positive signal caused by nonspecific amplification.[19] Thus, the construction of a rapid and sensitive biosensor is urgently needed for 8-oxoguanine DNA glycosylase assay.

Recently, the CRISPR-Cas system has become an emerging and powerful tool in genome editing, transcription regulation, and molecular diagnostics,[22−24] and it contains a guide RNA (gRNA) and a CRISPR-associated protein (Cas).[25] The

Received: October 14, 2021
Accepted: January 10, 2022
Published: January 20, 2022

https://doi.org/10.1021/acs.analchem.1c04453
Anal. Chem. 2022, 94, 2119−2125

CRISPR-Cas12 and CRISPR-Cas13 effectors exhibit target-activated, nonspecific collateral cleavage activity (indiscriminate hydrolysis of single-stranded DNA (ssDNA) or RNA) when the Cas−crRNA−target complex is formed, facilitating the construction of simple and sensitive biosensors.[26−28] To date, a variety of signal amplification strategies (e.g., RCA,[29,30] LAMP,[31] duplex-specific nuclease (DSN)-assisted signal amplification,[32] hybridization chain reaction (HCR),[33] and catalytic hairpin assembly (CHA)[34]) have been integrated with the CRISPR-Cas12 effector for the construction of various biosensors. Despite their good performance, these biosensors suffer from time-consuming reaction processes, multiple reaction procedures, and laborious washing/separation steps. Herein, we construct a CRISPR-Cas-based biosensor for sensitive and rapid measurement of both Fpg and hOGG1. In this strategy, we design a hairpin DNA as the SDA template to efficiently block the hybridization of the generated activators with free hairpin probes. When 8-oxoguanine DNA glycosylase is present, it removes the damaged 8-oxoG from the detection probe. The cleaved detection probe can function as a primer to start the quadratic SDA, generating a large number of activators. Subsequently, the activators can bind with crRNAs to activate Cas12a, cleaving signal probes and recovering Cy5 fluorescence. Single-molecule imaging is further employed to accurately quantify Cy5 fluorescent molecules. This biosensor can detect Fpg with a detection limit of 4.2×10^{-9} U μL^{-1} and accurately measure cellular hOGG1 at a single-cell level.

EXPERIMENTAL SECTION

General. The reagents and materials as well as cell culture and cell extracts preparation are described in the Supporting Information. All oligonucleotides (Table 1) were obtained from Sangon Biological Engineering Technology & Services Co., Ltd. (Shanghai, China).

Table 1. Sequences of Oligonucleotides[a]

note	sequence (5′−3′)
hairpin probe	C3 spacer-GTT ACC CTT ACC CTA GGC TGA GGA TCA CCG TAC TAG GGT AAG GGT AAC TAC GCT GAG GAT AAG TAC CAA CCA CCA CCC AGT CC-C3 spacer
detection probe	GGA CTG GGT GGT GGT TGO TAC TTA TCT TTT TTT T
activator	TCA GCC TAG GGT AAG GGT AAC
linear probe	C3 spacer-GTT ACC CTT ACC CTA GGC TGA GGA TGA CCG AAA CCG TAA CTA CGC TGA GGA TAA GTA CCA ACC ACC ACC CAG TCC-C3 spacer
crRNA	UAA UUU CUA CUA AGU GUA GAU ACC CUU ACC CUA GGC UGA
signal probe	Cy5-AAC CGC TTC CCC GAC TTC C-BHQ2

[a]In the detection probe, the underlined letter "O" indicates the oxidized guanine (8-oxoG).

Preparation of Hairpin Substrates. The hairpin substrates were obtained by hybridizing a 2 μM detection probe with a 2 μM hairpin probe in a buffer (1.5 mM $MgCl_2$,10 mM Tris−HCl, pH 8.0) at 95 °C for 5 min and subsequently cooling to room temperature.

Detection of 8-Oxoguanine DNA Glycosylase. The reaction was performed in 20 μL of a solution containing different concentrations of 8-oxoguanine DNA glycosylase, 10 nM hairpin substrates, 2 U of PNK, 5 U of Nt.BbvCI, 0.5 U of KF polymerase, 200 μM dNTPs, 50 nM Cas12a, 50 nM crRNA, 1.5 μM signal probe, and 1× NEBuffer 1.1 (10 mM $MgCl_2$, 100 μg mL^{-1} BSA, 10 mM bis-Tris-propane-HCl, pH 7.0) at 37 °C for 30 min, followed by termination at 65 °C for 10 min.

Fluorescence Measurements and Gel Electrophoresis. The fluorescence signals were measured with an FLS-1000 fluorescence spectrometer (Edinburgh Instruments Ltd., Livingston, U.K.) with 635 nm excitation. The 12% non-denaturing polyacrylamide gel electrophoresis (PAGE) was performed using SYBR Gold as an indicator. A ChemiDoc MP imaging system (Bio-Rad, Hercules, CA) was employed for gel imaging.

Single-Molecule Detection. Prior to single-molecule detection, the reaction products were diluted 19 000-fold with the imaging buffer (1 mM trolox, 12.5 mM $MgCl_2$, 10 mM Tris−HCl, pH 8.0). Then, 10 μL of the diluted samples was directly spread on a glass coverslip for total internal reflection fluorescence (TIRF) imaging. Cy5 fluorescent molecules were excited by a 640 nm laser. The photons from Cy5 were collected by a 100× oil immersion objective (NA 1.45, Olympus) and imaged by an EMCCD camera (Andor, Belfast, U.K.) with an exposure time of 500 ms. The Cy5 spots in a region of interest (ROI) of 600 × 600 pixels were counted using ImageJ software. The total Cy5 counts were obtained by calculating 10 frames. For the single-molecule photobleaching experiments, the diluted samples were continuously excited by a 640 nm laser, and the live images were collected at a high frequency with an exposure time of 400 ms. A total of 51 frames were collected and analyzed.

Inhibition Analysis. A DNA glycosylase inhibition assay was performed by incubating different concentrations of $CdCl_2$ with 1×10^{-5} U μL^{-1} Fpg in 1× NEBuffer 1.1 for 20 min at 37 °C, and the measurement of the Fpg activity followed the same procedures described above. The enzyme activity was obtained according to the linear correlation equation (Figure 2C). The relative activity of Fpg (RA) was measured on the basis of eq 1.

$$\mathrm{RA}\ (\%) = C_i/C_t \times 100\% = 10^{(N_i - N_t)/206.95} \times 100\% \quad (1)$$

where N_t and N_i are the Cy5 counts generated by Fpg and Fpg + $CdCl_2$, respectively.

RESULTS AND DISCUSSION

Principle of the CRISPR/Cas12a-Based Biosensor for 8-Oxoguanine DNA Glycosylase Assay. The principle of 8-oxoguanine DNA glycosylase detection is illustrated in Scheme 1. Both Fpg and hOGG1 are bifunctional DNA glycosylases with the functions of AP-lyase and *N*-glycosylase. The BER pathways for the repair of 8-oxoG are shown in Figure S1. This assay involves a hairpin probe, a detection probe, a signal probe, and a crRNA. The hairpin probe contains five regions including one binding region for the detection probe, two recognition regions for the Nt.BbvCI nicking enzyme, and two amplification regions for quadratic SDA reaction, with 5′- and 3′-ends of the hairpin probe being modified with C3 spacer (polymerase extension blocking group) to avoid the non-specific amplification.[35] The detection probe is labeled with an 8-oxoG base in the 18 nt site from the 5′ end. The hairpin substrate is formed by the hybridization of the detection probe with the hairpin probe. Notably, in comparison with a linear probe-based assay (Scheme S1), the introduction of a hairpin probe can efficiently block the hybridization of activators with free hairpin substrates (Figure S2), greatly improving the

https://doi.org/10.1021/acs.analchem.1c04453
Anal. Chem. 2022, 94, 2119−2125

Scheme 1. Principle of CRISPR-Cas-Based Biosensor for 8-Oxoguanine DNA Glycosylase Detection Based on the Integration of Target-Initiated Quadratic SDA with CRISPR/Cas12a Effector

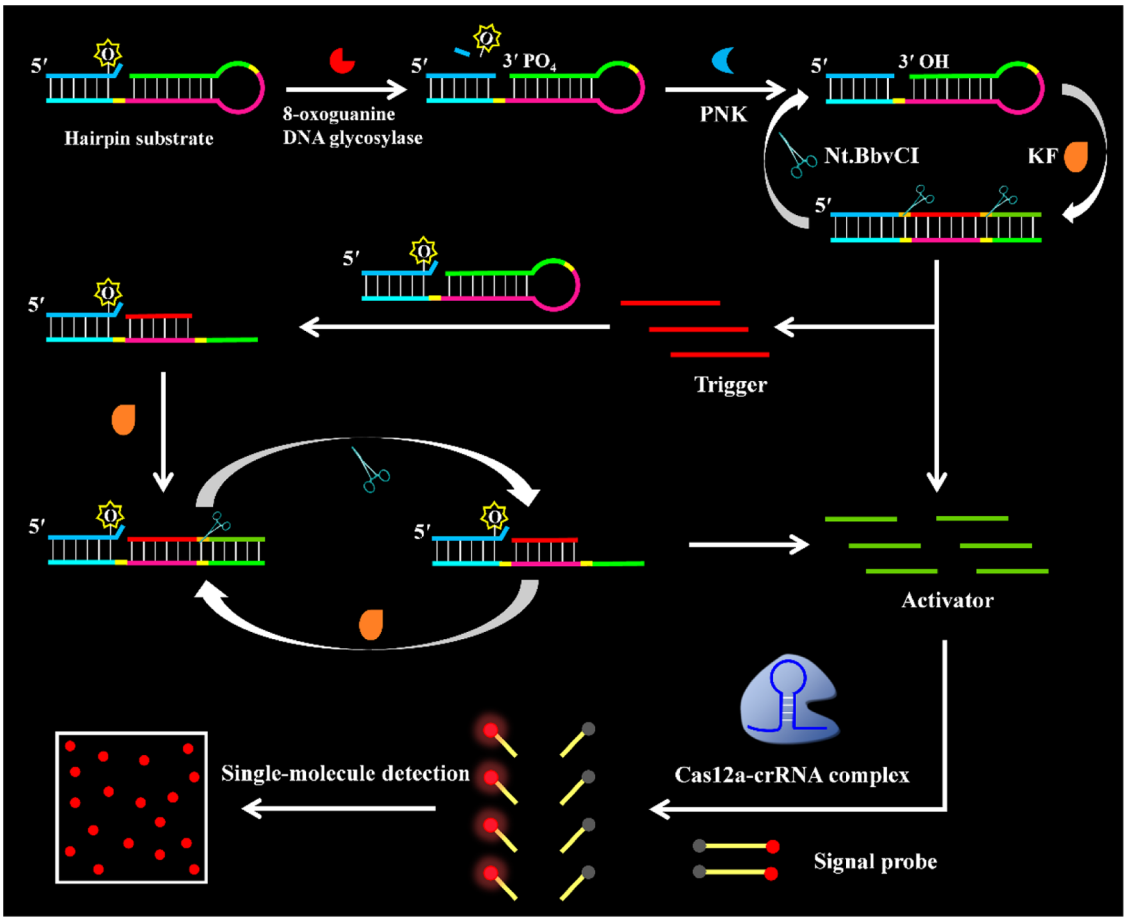

detection sensitivity. The signal probe is modified with a BHQ2 and a Cy5 at two ends, respectively, with Cy5 being quenched by BHQ2. This assay consists of four steps including (1) 8-oxoguanine DNA glycosylase-actuated 8-oxoG excision repair reaction, (2) enzyme-assisted quadratic SDA reaction, (3) CRISPR/Cas12a-catalyzed hydrolysis of signal probes, and (4) single-molecule imaging (Scheme 1). In the presence of 8-oxoguanine DNA glycosylase (e.g., Fpg), it can especially recognize the damaged 8-oxoG in hairpin substrates and remove it from the 8-oxoG:C pairs, leaving a single-nucleotide gap.[13,36] PNK can catalyze the 3′-phosphate group of the resultant gap site to produce free 3′-OH termini.[13,37] Notably, we employed PNK rather than apurinic/apyrimidinic endonuclease (APE1) to detect Fpg with only a one-step reaction because PNK can achieve much better assay performance than APE1 under identical conditions (Figure S3). With the assistance of dNTPs and Klenow fragment DNA polymerase, the free 3′-OH-containing detection probe can act as the primer to initiate polymerization extension, unfolding the hairpin probe and eventually forming a double-stranded DNA (dsDNA) that contains two recognition sites for Nt.BbvCI (Scheme 1, yellow/orange color). The subsequent cleavage of the upper DNA strand by the Nt.BbvCI enzyme generates two new replication sites for DNA polymerase, inducing the first SDA with the assistance of Nt.BbvCI enzyme and Klenow fragment DNA polymerase to generate abundant triggers and activators. The hybridization of triggers with new hairpin probes can initiate the second cyclic polymerization−nicking−displacement to produce more and more activators. The binding of activators with crRNA can activate Cas12a, leading to the cleavage of signal probes, releasing abundant Cy5 molecules. In contrast, the absence of Fpg cannot induce the removal of the 8-oxoG base, and neither the initiation of quadratic SDA reaction nor the generation of activators can occur. As a result, CRISPR/Cas12a cannot be activated and no Cy5 signal is observed.

Validation of the Assay. The reaction products are characterized by a 12% nondenaturing PAGE (Figure 1A). A distinct band of activator/crRNA hybrids (Figure 1A, lane 1, green color) with the same length as the synthesized activator/crRNA hybrids (Figure 1A, lane 3, green color) is detected, indicating the initiation of a quadratic SDA reaction by Fpg. Meanwhile, the cleavage of Cy5-labeled signal probes generates distinct fluorescent bands (Figure 1A, lane 1, red color), indicating that the activators generated from the quadratic SDA reaction can activate the *trans*-cleavage activity of CRISPR/Cas12a. When Fpg is absent, no distinct band is detected (Figure 1A, lane 2), suggesting that neither the quadratic SDA reaction nor the initiation of CRISPR/Cas12a can occur. We further performed the fluorescence measurements (Figure 1B). A high Cy5 signal is detected when Fpg is present (Figure 1B, red color), but no significant Cy5 signal is observed when Fpg is absent (Figure 1B, blue color), identical to that of control without Fpg and PNK (Figure 1B, black color).

https://doi.org/10.1021/acs.analchem.1c04453
Anal. Chem. 2022, 94, 2119−2125

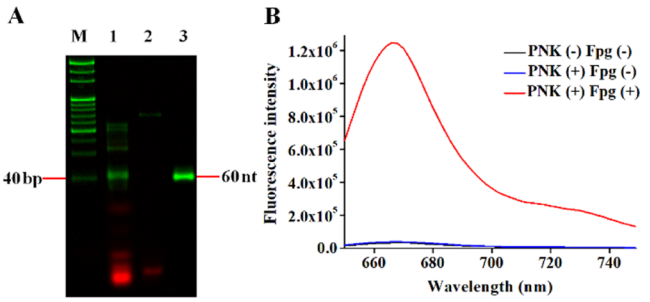

Figure 1. (A) Nondenaturing PAGE analysis of reaction products. Lane 1, with Fpg; lane 2, without Fpg; lane 3, with the synthesized activator/crRNA hybrids; lane M, 20 bp DNA ladder marker. The 0.01 U μL^{-1} Fpg, 150 nM synthesized activator/crRNA hybrids, and 1.5 μM signal probe were employed in the experiments. (B) Fluorescence emission spectra in response to PNK (blue color), PNK + Fpg (red color), and the control with the absence of Fpg and PNK (black color). 0.01 U μL^{-1} Fpg and 0.1 U μL^{-1} PNK were employed in the experiments.

Single-Molecule Detection. 8-Oxoguanine DNA glycosylase activity is detected by single-molecule imaging (Figure 2). When Fpg is present, it generates distinct Cy5 fluorescence signals (Figure 2A), suggesting that Fpg can recognize and remove the damaged 8-oxoG with the assistance of PNK and initiate the subsequent quadratic SDA reaction and CRISPR/Cas12a-catalyzed cleavage reaction. On the contrary, the absence of Fpg generates a near-zero background signal (Figure 2B), indicating that neither quadratic SDA reaction nor CRISPR/Cas12a-catalyzed cleavage reaction occurs. Notably, Cy5 fluorescent spots in the single-molecule fluorescence image exhibit one-step photobleaching (Figure S4), indicating that the detected spots represent a single Cy5 molecule.

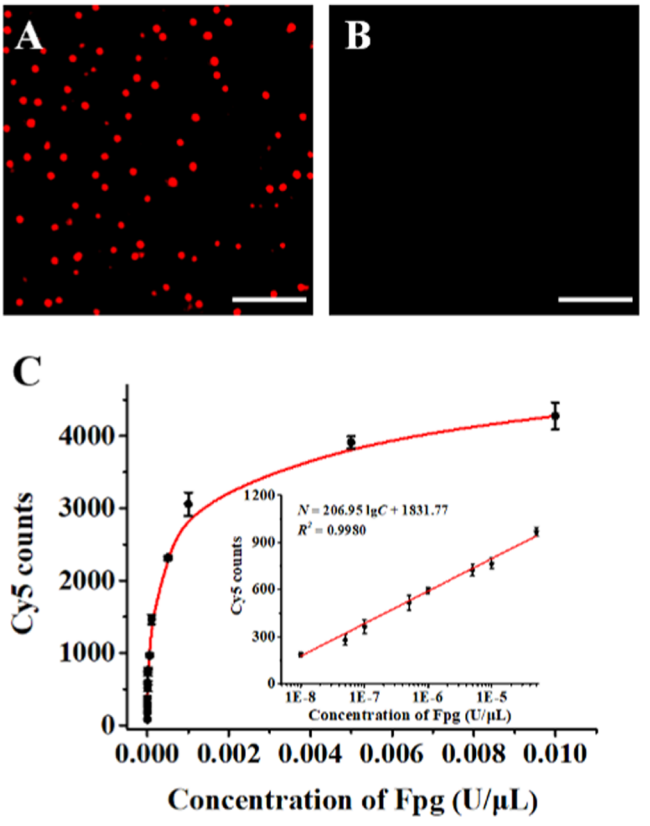

Figure 2. (A, B) Single-molecule images of Cy5 in the presence (A) and absence (B) of Fpg (0.01 U μL^{-1}). The scale bar is 5 μm. (C) Cy5 counts induced by different concentrations of Fpg. Inset shows the linear increase in Cy5 counts with Fpg concentration in the logarithmic scale.

Detection Sensitivity. We study the influence of Fpg concentration on the Cy5 counts under optimal conditions (Figures S5 and S6). Fpg induces a concentration-dependent increase in Cy5 counts (Figure 2C). In a logarithmic scale, the Cy5 counts (N) linearly improve with Fpg concentration (C) in the range from 1×10^{-8} to 5×10^{-5} U μL^{-1} (inset of Figure 2C), with the corresponding equation being $N = 1831.77 + 206.95 \lg C$ ($R^2 = 0.9980$). The limit of detection (LOD) of 4.24×10^{-9} U μL^{-1} is obtained. In comparison with the reported methods, this biosensor is characterized by shorter analysis time, fewer experimental steps, and a lower detection limit (Table S1).[19−21,38−42] The high sensitivity may be attributed to four factors: (1) high amplification efficiency of quadratic SDA induced by Fpg-catalyzed 8-oxoG excision repair, (2) efficient blocking of the hybridization of activators with free hairpin probes induced by the introduction of a hairpin structure, and (3) signal amplification induced by the activator/crRNA/Cas12a complex-driven recycle cleavage of signal probes, and (4) high sensitivity of single-molecule imaging.

Detection Specificity. We select human alkyladenine DNA glycosylase (hAAG), immunoglobulin G (IgG), uracil DNA glycosylase (UDG), and bovine serum albumin (BSA) as interferences. Only Fpg can generate a high Cy5 signal (Figure 3, violet color). In contrast, BSA (Figure 3, orange color), IgG (Figure 3, green color), UDG (Figure 3, blue color), and hAAG (Figure 3, cyan color) cannot generate a significant Cy5 signal. Moreover, the addition of Fpg to the interferents generates a high Cy5 signal (Figure 3, red color) identical to that generated by 0.01 U μL^{-1} Fpg (Figure 3, violet color), further confirming the good selectivity of this biosensor.

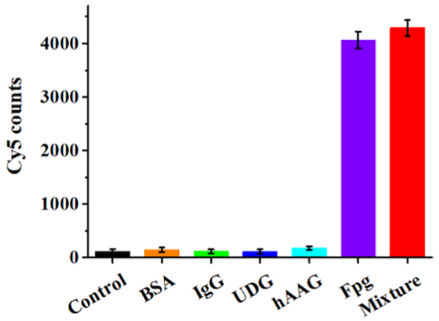

Figure 3. Cy5 counts induced by 0.1 mg mL^{-1} BSA (orange color), 0.01 U μL^{-1} UDG (blue color), 0.01 U μL^{-1} hAAG (cyan color), 0.1 mg mL^{-1} IgG (green color), 0.01 U μL^{-1} Fpg (violet color), mixture of 0.01 U μL^{-1} Fpg + all above interferences (red color), and the reaction buffer (control, black color), respectively.

Inhibition Assay. Chromium(II) chloride ($CdCl_2$) is selected as the inhibitor for the inhibition assay. $CdCl_2$ can inhibit the DNA substrate cleavage via the binding of Cd^{2+} with the DNA glycosylase substrate and inactivate the catalytic activity via direct binding of Cd^{2+} with the active site of DNA glycosylase.[43] Notably, Cd^{2+} does not inhibit the activities of the other four enzymes in the system except for Fpg (Figure S7). As shown in Figure 4A, $CdCl_2$ induces a decrease in the

https://doi.org/10.1021/acs.analchem.1c04453
Anal. Chem. 2022, 94, 2119−2125

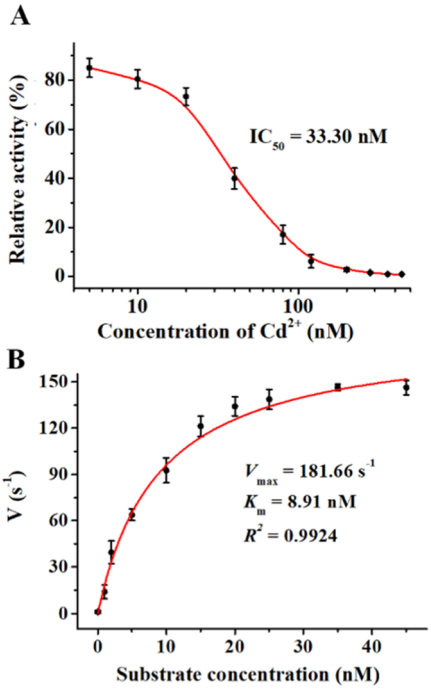

Figure 4. (A) $CdCl_2$ induces a concentration-dependent decrease in the Fpg relative activity. The Fpg concentration is 1×10^{-5} U μL^{-1}. (B) Change in initial velocity (V) as a function of DNA substrate concentration. The Fpg concentration is 0.01 U μL^{-1}.

Fpg relative activity in a concentration-dependent manner. The IC_{50} value of 33.3 nM is obtained. This result suggests the potential of this biosensor for drug discovery.

Kinetic Analysis. The kinetic parameters of Fpg are obtained by measuring the initial velocity at 37 °C in a 5 min reaction. The initial velocity increases as a function of DNA substrate concentration (Figure 4B). The kinetic parameters including Michaelis–Menten constant K_m and the maximum initial velocity V_{max} can be calculated based on the Michaelis–Menten equation (eq 2).

$$V = V_{max}[S]/(K_m + [S]) \quad (2)$$

where [S] is the DNA substrate concentration and V is the initial velocity. The K_m and V_{max} are determined as 8.91 nM and 181.66 s^{-1}, respectively. Notably, the obtained K_m value is consistent with that measured using gel electrophoresis (K_m = 8.9 nM).[44]

Detection of Cellular hOGG1. To evaluate the effect of nuclear matrix upon the detection system, we perform the recovery studies by spiking different concentrations of Fpg into the inactivated A549 cell nuclear extracts. The recovery ratio is determined as 97.40–98.17% with a relative standard deviation (RSD) of 1.93–2.58% (Table S2), suggesting the excellent performance of this method in a complex nuclear matrix. To demonstrate the generality of this biosensor, we use this biosensor to detect the cellular hOGG1 activity in the human lung adenocarcinoma cell line (A549 cells). The whole-cell extracts (Figure 5A, red color) and nucleus (Figure 5A, blue color) generate high fluorescence signals, but the cytoplasm extracts (Figure 5A, violet color) generate no significant fluorescence signal, suggesting the main location of hOGG1 in the nucleus, consistent with the previous research.[45] Moreover, the higher the number of A549 cells, the higher the Cy5 counts measured (Figure 5B). In the logarithmic scale, the Cy5 counts (N) increase linearly with the numbers of A549 cells (X) in the range of 1–100 cells (Figure 5C), with the equation being $N = 206.95 \lg X - 1831.77$ (R^2 = 0.9980). Notably, this biosensor can measure endogenous 8-oxoguanine DNA glycosylase

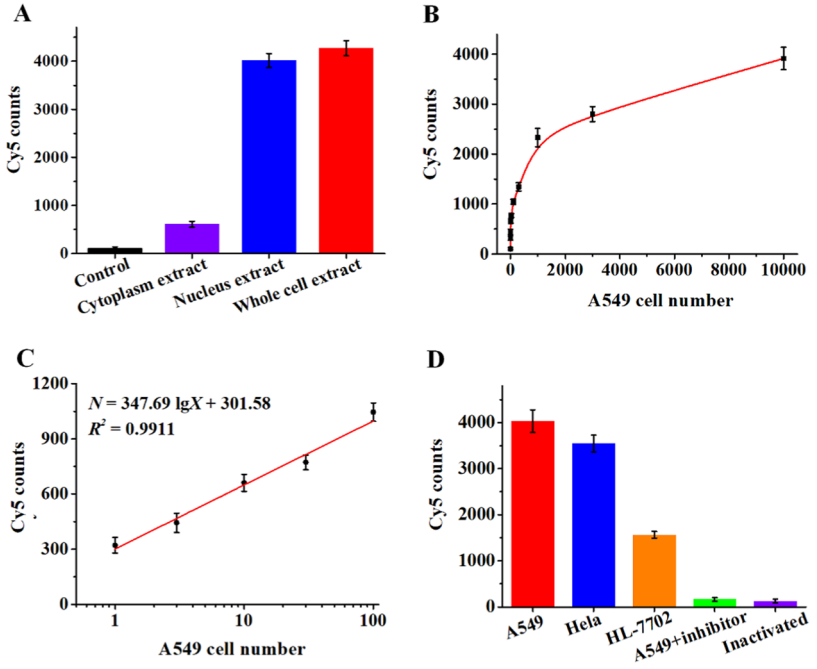

Figure 5. (A) Cy5 counts induced by the cytoplasm (violet color), nucleus (blue color), and whole-cell extracts (red color) from 10 000 A549 cells and the control (black color). (B) Variance in Cy5 counts as a function of the number of A549 cells. (C) Linear dependence of Cy5 counts upon the logarithm of the number of A549 cells ranging from 1 to 100 cells. (D) Measurement of Cy5 counts generated by HL-7702 cells (orange color), A549 cells (red color), HeLa cells (blue color), A549 cells + Cd^{2+} (green color), and inactivated A549 cell extracts (violet color).

https://doi.org/10.1021/acs.analchem.1c04453
Anal. Chem. 2022, 94, 2119–2125

activity equivalent to 1 cell, indicating the capability of this biosensor to detect cellular hOGG1 with single-cell sensitivity.

We further measured 8-oxoguanine DNA glycosylase activity in human hepatocyte cell line (HL-7702 cells), human cervical carcinoma cell line (HeLa cells), and A549 cells (Figure 5D), respectively. A549 cells (Figure 5D, red color) and HeLa cells (Figure 5D, blue color) can produce significantly high Cy5 counts, which is consistent with the high glycosylase activity in cancer cells.[46] In contrast, HL-7702 cells (Figure 5D, orange color) generate no significant Cy5 counts, suggesting the low 8-oxoguanine DNA glycosylase activity in normal cells. Notably, no significant Cy5 counts are detected upon either the heat treatment (Figure 5D, violet color) or the incubation of A549 cells with $CdCl_2$ (Figure 5D, green color), which can induce the loss of glycosylases activity.

CONCLUSIONS

We have constructed a CRISPR-Cas-based biosensor for rapid and sensitive detection of both Fpg and hOGG1. This biosensor involves a hairpin probe and integrates quadratic SDA with the CRISPR/Cas12a effector. The presence of 8-oxoguanine DNA glycosylase can initiate the quadratic SDA to produce large amounts of activators with the assistance of PNK. The designed hairpin probes can effectively block the hybridization of the generated activators with free hairpin probes, making all activators bind with crRNAs to activate Cas12 and endowing this biosensor with high sensitivity. Moreover, hairpin probes modified with C3 spacer can efficiently prevent nonspecific amplification, endowing this biosensor with high specificity. In addition, the utilization of PNK instead of APE1 greatly simplifies the experimental procedure with only a one-step reaction. Even though this biosensor involves three consecutive reactions including the base excision reaction, quadratic SDA reaction, and CRISPR/Cas12a-catalyzed cleavage reaction, three reactions can be well combined into a one-step reaction with excellent performance. This biosensor possesses the characteristics of rapidity (within 40 min) and isothermal assay, without the requirement of any complex immobilization/separation steps and time-consuming preparation of functional nanomaterials. Especially, the introduction of single-molecule detection further reduces the sample consumption and improves the detection sensitivity. This biosensor can detect Fpg with a LOD of 4.24×10^{-9} U μL^{-1} and accurately measure cellular hOGG1 with single-cell sensitivity. Moreover, this biosensor can be used for the screening of inhibitors, the analysis of kinetic parameters, and the discrimination of cancer cells from normal cells, with potential applications in molecular diagnostic and point-of-care testing.

ASSOCIATED CONTENT

Supporting Information

The Supporting Information is available free of charge at https://pubs.acs.org/doi/10.1021/acs.analchem.1c04453.

Chemicals and materials, cell culture and cell extract preparation, schematic representation of three BER subpathways for the repair of 8-oxoG in human cells, comparison of the performance of hairpin probe with linear probe, comparison of the performance of PNK with APE1, single-molecule stepwise photobleaching trajectory over time for individual Cy5 molecule, optimization of experimental conditions, assessment of the effect of Cd^{2+} upon the activities of other four enzymes in the system, comparison of this strategy with the reported methods for 8-oxoguanine DNA glycosylase assay, and recovery studies by spiking Fpg into the inactivated A549 cell nuclear extracts (PDF)

AUTHOR INFORMATION

Corresponding Authors

Jian-Ge Qiu − *Academy of Medical Sciences, Zhengzhou University, Zhengzhou 450000 Henan, China*; Email: jiangeqiu@zzu.edu.cn

Chun-yang Zhang − *College of Chemistry, Chemical Engineering and Materials Science, Shandong Normal University, Jinan 250014, China*; orcid.org/0000-0002-8010-1981; Phone: +86 0531-86186033; Email: cyzhang@sdnu.edu.cn; Fax: +86 0531-82615258

Authors

Qian Zhang − *College of Chemistry, Chemical Engineering and Materials Science, Shandong Normal University, Jinan 250014, China*

Shuangnan Zhao − *College of Chemistry, Chemical Engineering and Materials Science, Shandong Normal University, Jinan 250014, China*

Xiaorui Tian − *College of Chemistry, Chemical Engineering and Materials Science, Shandong Normal University, Jinan 250014, China*

Complete contact information is available at: https://pubs.acs.org/10.1021/acs.analchem.1c04453

Author Contributions

§Q.Z., S.Z., and X.T. contributed equally.

Notes

The authors declare no competing financial interest.

ACKNOWLEDGMENTS

This work was supported by the National Natural Science Foundation of China (grant nos. 21735003, 21527811, and 21705096) and the Award for Team Leader Program of Taishan Scholars of Shandong Province, China.

REFERENCES

(1) David, S. S.; O'Shea, V. L.; Kundu, S. *Nature* **2007**, *447*, 941−950.

(2) Schärer, O. D. *Angew. Chem., Int. Ed.* **2003**, *42*, 2946−2974.

(3) Wang, J.; Yuan, B.; Guerrero, C.; Bahde, R.; Gupta, S.; Wang, Y. *Anal. Chem.* **2011**, *83*, 2201−2209.

(4) Liu, Y.; Wei, M.; Zhang, L.; Zhang, Y.; Wei, W.; Yin, L.; Pu, Y.; Liu, S. *Anal. Chem.* **2016**, *88*, 6509−6514.

(5) Shibutani, S.; Takeshita, M.; Grollman, A. P. *Nature* **1991**, *349*, 431−434.

(6) Fukae, J.; Takanashi, M.; Kubo, S.; Nishioka, K.; Nakabeppu, Y.; Mori, H.; Mizuno, Y.; Hattori, N. *Acta Neuropathol.* **2005**, *109*, 256−262.

(7) Bashir, S.; Harris, G.; Denman, M. A.; Blake, D. R.; Winyard, P. G. *Ann. Rheum. Dis.* **1993**, *52*, 659−666.

(8) Yuzefovych, L. V.; Kahn, A. G.; Schuler, M. A.; Eide, L.; Arora, R.; Wilson, G. L.; Tan, M.; Rachek, L. I. *Cancer Res.* **2016**, *76*, 30−34.

(9) Chevillard, S.; Radicella, J. P.; Levalois, C.; Lebeau, J.; Poupon, M. F.; Oudard, S.; Dutrillaux, B.; Boiteux, S. *Oncogene* **1998**, *16*, 3083−3086.

(10) Elahi, A.; Zheng, Z.; Park, J.; Eyring, K.; McCaffrey, T.; Lazarus, P. *Carcinogenesis* **2002**, *23*, 1229−1234.

(11) Obtulowicz, T.; Swoboda, M.; Speina, E.; Gackowski, D.; Rozalski, R.; Siomek, A.; Janik, J.; Janowska, B.; Ciesla, J. M.; Jawien, A.; Banaszkiewicz, Z.; Guz, J.; Dziaman, T.; Szpila, A.; Olinski, R.; Tudek, B. *Mutagenesis* **2010**, *25*, 463−471.
(12) Shinmura, K.; Kohno, T.; Kasai, H.; Koda, K.; Sugimura, H.; Yokota, J. *Jpn. J. Cancer Res.* **1998**, *89*, 825−828.
(13) Boiteux, S.; Coste, F.; Castaing, B. *Free Radical Biol. Med.* **2017**, *107*, 179−201.
(14) Zhang, Y.; Hua, R. N.; Zhang, C. Y. *Anal. Chem.* **2019**, *91*, 10381−10385.
(15) Grin, I. R.; Konorovsky, P. G.; Nevinsky, G. A.; Zharkov, D. O. *Biochemistry* **2009**, *74*, 1253−1259.
(16) Darwanto, A.; Farrel, A.; Rogstad, D. K.; Sowers, L. C. *Anal. Biochem.* **2009**, *394*, 13−23.
(17) Ma, L.; Chu, H.; Wang, M.; Shi, D.; Zhong, D.; Li, P.; Tong, N.; Yin, C.; Zhang, Z. *Cancer Sci.* **2012**, *103*, 1215−1220.
(18) Gackowski, D.; Speina, E.; Zielinska, M.; Kowalewski, J.; Rozalski, R.; Siomek, A.; Paciorek, T.; Tudek, B.; Olinski, R. *Cancer Res.* **2003**, *63*, 4899−4902.
(19) Wang, X.; Hou, T.; Lu, T.; Li, F. *Anal. Chem.* **2014**, *86*, 9626−9631.
(20) Wang, L. J.; Lu, Y. Y.; Zhang, C. Y. *Chem. Sci.* **2020**, *11*, 587−595.
(21) Kong, X. J.; Wu, S.; Cen, Y.; Yu, R. Q.; Chu, X. *Biosens. Bioelectron.* **2016**, *79*, 679−684.
(22) Gilbert, L. A.; Larson, M. H.; Morsut, L.; Liu, Z.; Brar, G. A.; Torres, S. E.; Stern-Ginossar, N.; Brandman, O.; Whitehead, E. H.; Doudna, J. A.; Lim, W. A.; Weissman, J. S.; Qi, L. S. *Cell* **2013**, *154*, 442−451.
(23) Shan, Y.; Zhou, X.; Huang, R.; Xing, D. *Anal. Chem.* **2019**, *91*, 5278−5285.
(24) Wang, G.; Tian, W.; Liu, X.; Ren, W.; Liu, C. *Anal. Chem.* **2020**, *92*, 6702−6708.
(25) Ran, F. A.; Hsu, P. D.; Wright, J.; Agarwala, V.; Scott, D. A.; Zhang, F. *Nat. Protoc.* **2013**, *8*, 2281−2308.
(26) Chen, J. S.; Ma, E.; Harrington, L. B.; Da Costa, M.; Tian, X.; Palefsky, J. M.; Doudna, J. A. *Science* **2018**, *360*, 436−439.
(27) Gootenberg, J. S.; Abudayyeh, O. O.; Lee, J. W.; Essletzbichler, P.; Dy, A. J.; Joung, J.; Verdine, V.; Donghia, N.; Daringer, N. M.; Freije, C. A.; Myhrvold, C.; Bhattacharyya, R. P.; Livny, J.; Regev, A.; Koonin, E. V.; Hung, D. T.; Sabeti, P. C.; Collins, J. J.; Zhang, F. *Science* **2017**, *356*, 438−442.
(28) Wang, B.; Wang, R.; Wang, D.; Wu, J.; Li, J.; Wang, J.; Liu, H.; Wang, Y. *Anal. Chem.* **2019**, *91*, 12156−12161.
(29) Tian, W.; Liu, X.; Wang, G.; Liu, C. *Chem. Commun.* **2020**, *56*, 13445−13448.
(30) Qing, M.; Chen, S. L.; Sun, Z.; Fan, Y.; Luo, H. Q.; Li, N. B. *Anal. Chem.* **2021**, *93*, 7499−7507.
(31) Zhang, M.; Wang, H.; Wang, H.; Wang, F.; Li, Z. *Anal. Chem.* **2021**, *93*, 7942−7948.
(32) Li, J.; Yang, S.; Zuo, C.; Dai, L.; Guo, Y.; Xie, G. *ACS Sens.* **2020**, *5*, 970−977.
(33) Kachwala, M. J.; Smith, C. W.; Nandu, N.; Yigit, M. V. *Anal. Chem.* **2021**, *93*, 1934−1938.
(34) Peng, S.; Tan, Z.; Chen, S.; Lei, C.; Nie, Z. *Chem. Sci.* **2020**, *11*, 7362−7368.
(35) Uren, A. G.; Mikkers, H.; Kool, J.; van der Weyden, L.; Lund, A. H.; Wilson, C. H.; Rance, R.; Jonkers, J.; van Lohuizen, M.; Berns, A.; Adams, D. J. *Nat. Protoc.* **2009**, *4*, 789−798.
(36) Czene, S.; Harms-Ringdahl, M. *Mutat. Res., DNA Repair* **1995**, *336*, 235−242.
(37) Wiederhold, L.; Leppard, J. B.; Kedar, P.; Karimi-Busheri, F.; Rasouli-Nia, A.; Weinfeld, M.; Tomkinson, A. E.; Izumi, T.; Prasad, R.; Wilson, S. H.; Mitra, S.; Hazra, T. K. *Mol. Cell* **2004**, *15*, 209−220.
(38) Yuan, F.; Zhao, H.; Liu, M.; Quan, X. *Biosens. Bioelectron.* **2015**, *68*, 7−13.
(39) Wu, Z.; Wu, Z. K.; Tang, H.; Tang, L. J.; Jiang, J. H. *Anal. Chem.* **2013**, *85*, 4376−4383.
(40) Hu, J.; Liu, M. H.; Li, Y.; Tang, B.; Zhang, C. Y. *Chem. Sci.* **2018**, *9*, 712−720.
(41) Wang, L. J.; Wang, H. X.; Jiang, L.; Zhang, C. Y. *ACS Sens.* **2018**, *3*, 2675−2683.
(42) Wang, L.-J.; Liang, L.; Liu, B.-J.; Jiang, B.; Zhang, C.-Y. *Chem. Sci.* **2021**, *12*, 5544−5554.
(43) Zharkov, D. O.; Rosenquist, T. A. *DNA Repair* **2002**, *1*, 661−670.
(44) Hill, J. W.; Hazra, T. K.; Izumi, T.; Mitra, S. *Nucleic Acids Res.* **2001**, *29*, 430−438.
(45) Bohr, V. A. *Free Radicals Biol. Med.* **2002**, *32*, 804−812.
(46) Leitner-Dagan, Y.; Sevilya, Z.; Pinchev, M.; Kramer, R.; Elinger, D.; Roisman, L. C.; Rennert, H. S.; Schechtman, E.; Freedman, L.; Rennert, G.; Livneh, Z.; Paz-Elizur, T. *JNCI, J. Natl. Cancer Inst.* **2012**, *104*, 1765−1769.

https://doi.org/10.1021/acs.analchem.1c04453
Anal. Chem. 2022, 94, 2119−2125